Field Determination of Linear and Nonlinear Constrained Moduli of Soils Using Large Mobile Shakers

M.T. LeBlanc & K.H. Stokoe, II
The University of Texas at Austin, Texas, United States

A.G. Branco, III
820th Red Horse Squadron, Nevada, United States

R.C. Lee
Los Alamos National Laboratory, New Mexico, United States

SUMMARY:
Within the last few years, a field method was developed to evaluate the linear and nonlinear shear moduli of soils using large mobile shakers. The present study was undertaken to determine if this field method could be extended to evaluating linear and nonlinear constrained moduli of soils. To this end, a vertical array of three, 3-D geophones was constructed in a relatively homogeneous sandy silt (ML) deposit. Linear and nonlinear wave propagation tests were then performed using a nees@UTexas vibroseis (large mobile shaker) to induce ground motions directly above the array. These tests were followed by traditional transient, small-strain downhole tests. The dynamic loading created vertically propagating constrained compression (P_v) waves. Constrained moduli (M) were calculated using P_v-wave velocities measured between adjacent geophones. The variation of M with axial strain was determined at several confining pressures over an axial strain range of 0.0004% to 0.03%. The variation of M with axial strain was quite complex. At the lowest pressure of about 20 kPa, M increased with increasing axial strain. At higher pressures, this trend decreased, but coupled nonlinearity and degradation began to occur. Further studies are needed.

Keywords: constrained modulus, nonlinear field measurements, large steady-state shaking

1. INTRODUCTION

Field seismic measurements have been performed for more than 50 years to determine the small-strain shear and constrained moduli of geotechnical materials. In recent years, a methodology was developed to characterize the linear and nonlinear shear moduli (G) of geotechnical materials in-situ. This approach involves application of static and dynamic loads from large mobile shakers at the ground surface and measurement of the response beneath the loaded area using embedded geophone sensors. This method was shown to be effective in characterizing the linear and nonlinear shear moduli of soils in-situ (Stokoe et al. 2006; Park 2010). Although in-situ measurements of linear and nonlinear shear moduli have been studied, in-situ measurements of linear and nonlinear constrained moduli (M) of soil have received little attention. The present research was undertaken to determine whether the in-situ techniques used to measure shear moduli can be extended to constrained moduli.

A new methodology for measuring linear and nonlinear constrained moduli of in-situ soil is presented in this paper. The field experimental set-up and data analysis procedures are discussed. Linear and nonlinear constrained modulus measurements are presented to show the feasibility of the method. Comparisons are made between the nonlinear constrained modulus curves and recent published shear modulus reduction curves for sandy silt.

2. EXPERIMENTAL PROGRAM

The experimental program involved three sequential steps: (1) fabrication, calibration, and installation of three-dimensional (3-D) geophone sensors, (2) steady-state dynamic wave velocity measurements

using a vibroseis called “Thumper,” and (3) traditional transient, small-strain downhole seismic tests.

2.1. Sensor Fabrication, Calibration, and Installation

The instrumentation consisted of 3, three-dimensional (3-D) sensors. Each 3-D sensor was fabricated in the laboratory using 3, one-dimensional, 28-Hz geophones (velocity transducers) aligned to capture dynamic motions in the three Cartesian directions (x-, y-, and z-directions). Each 3-D sensor was cast in epoxy resin, with design goals that the total unit weight of the 3-D sensor be equal to that of the in-situ soil and to ensure that the 3-D sensor acted as a rigid body. After fabrication, each 3-D sensor was calibrated in the laboratory using a shake table. During calibration, the voltage output of every geophone was recorded for known vibrational levels over frequencies from 1 to 300 Hz. The calibration tests yielded geophone calibration factors that were used to convert geophone output voltage to particle velocity at the measurement locations. For the 9, 1-D geophones, the calibration factors ranged from 0.118 to 0.150 V/(cm/sec) and averaged 0.141 V/(cm/sec) over the frequency range of 30 to 100 Hz. This frequency range covers all seismic measurements in this study.

After calibration, the 3-D sensors were installed at the field site in a vertical array as shown in Figure 1. The field site was located on a historical farm field near Hornsby Bend in Austin, Texas. The farm field had been ploughed in the preceding decades, leaving plough tillage (with topsoil and rocks) at the ground surface. An area large enough for the loading platens (a concrete footing and the vibroseis load plate) was scarified by hand to reach native sandy silt (ML) at a depth of approximately 17.8 cm. The soil at this depth had a total unit weight of approximately 18.9 kN/m^3 and a water content of 4 to 5%. A hand auger was used to drill a 6.4-cm diameter borehole to a depth of about 66 cm. The bottom of the borehole was prepared, and Sensor 3 was placed using an installation/orientation tool. The borehole was then backfilled with native soil and compacted until the desired depth for Sensor 2 was reached. Great care was taken to compact the backfilled soil to the same density as the in-situ soil. Sensor 2 was then installed, and the process was repeated to install Sensor 1. After Sensor 1 was installed, the remainder of the borehole was backfilled and compacted. The depths of the midpoints of the three sensors were 24.8, 45.1, and 65.4 cm, measured from the scarified soil surface (see Figure 1). Finally, a 2.5-cm deep layer of poorly graded sand was placed over the scarified surface to improve contact between a concrete footing or the vibroseis load plate and the ground surface during testing.

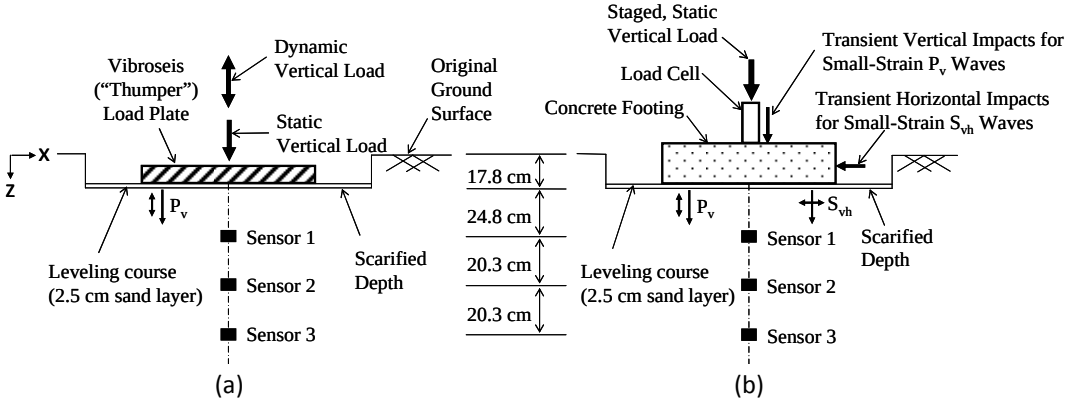

Figure 1. Field configuration for: (a) steady-state dynamic tests and (b) transient, small-strain seismic tests

2.2. Steady-State Dynamic and Transient, Small-Strain Wave Velocity Measurements

After the vertical sensor array was constructed, the soil mass was subjected to two stages of tests: (1) steady-state dynamic tests encompassing linear and nonlinear strain levels and (2) traditional transient, downhole seismic tests at small strains. The generalized two-stage test sequence is shown in Figure 2. Due to scheduling conflicts with the vibroseis, the transient, small-strain downhole tests were not performed before the steady-state dynamic tests, as would normally be the case. To characterize linear

and nonlinear constrained moduli, steady-state dynamic tests (Stage 1 in Figure 2) were performed using a vibroseis (large mobile shaker called "Thumper") with a 0.91-m diameter baseplate positioned over the sensor array as shown in Figure 1a. To limit the effects of the loading regimen on the underlying soil structure, a 4-stepped loading sequence was used in Stage 1. In each step, the mobile shaker applied a constant static load while the dynamic load was varied. Static loads ranged from 9 to 45 kN and peak dynamic loads ranged from 1 to 27 kN. At each dynamic load, a total of 10 cycles of sinusoidal shaking was imparted at various frequencies. Driving frequencies from 30 to 100 Hz were used and were selected such that the received waveforms from the geophones were clear. The "Thumper" vibroseis (shown in Figure 3) was provided by the nees@UTexas Equipment Site. The nees@UTexas Equipment Site is part of the George E. Brown, Jr. Network for Earthquake Engineering Simulations (NEES) with funding provided by the U.S. National Science Foundation (Stokoe et al. 2004).

Small-strain, transient seismic tests were performed in Stage 2 (see Figure 2) one week after Stage 1 was completed. A 5-stepped sequence of static vertical loads was applied to a 0.91-m diameter precast concrete footing positioned over the sensor array as shown in Figure 1b. The vertical load was increased (therefore increasing the vertical normal stress, σ_v) by jacking against the dead weight of the vibroseis. The impact from an instrumented hammer was used as the wave source, and the embedded sensors served as downhole receivers. The top of the concrete footing was struck directly with the instrumented hammer to generate vertically-propagating constrained compression (P_v) waves, and the side of the concrete footing was struck to generate vertically-propagating, horizontally-polarized shear (S_{vh}) waves (note that the behavior of the S_{vh} waves is not presented in this paper). The purposes of these tests were: (1) to confirm that the steady-state dynamic tests were measuring the P_v-wave velocity (V_{Pv}) and (2) to determine the log V_{Pv} – log σ_v relationship.

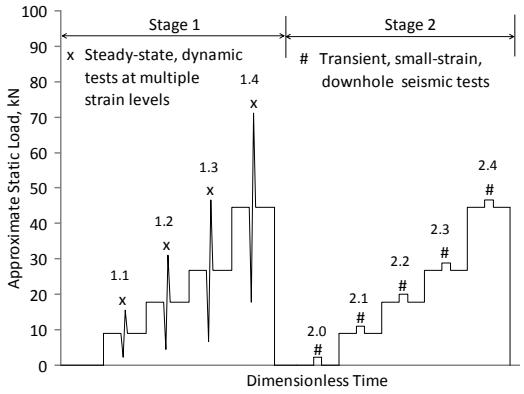

Figure 2. Generalized stage loading sequence (after Stokoe et al. 2006)

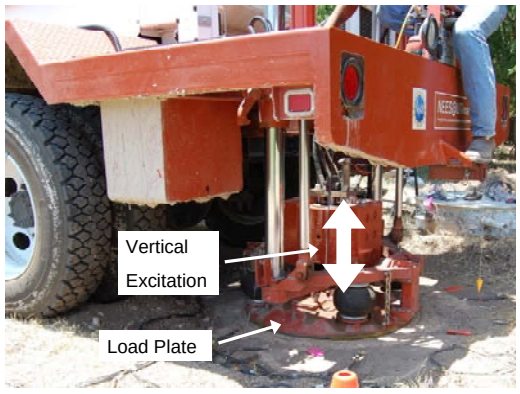

Figure 3. Load plate of the vibroseis called "Thumper" positioned over the embedded vertical sensor array

3. ANALYSIS PROCEDURES

The data analysis followed the procedures outlined by Stokoe et al. (2006) and Park (2010). The increase in vertical stress, $\Delta\sigma_v$, mid-way between each receiver pair that was induced by the static load of the mobile shaker was determined using a Boussinesq-based stress distribution for a circular foundation. Example calculations of transient, small-strain wave velocity and steady-state, dynamic linear and nonlinear wave velocity are given below. A discussion of the displacement-based method used to determine axial strain is also presented.

3.1. P_v-Wave Velocities from Transient, Small-Strain Tests Under Varying Static Loads

P_v waves under each static load step in Stage 2 (see Figure 2) were generated by a downward hammer

impact on the concrete footing. The small-strain V_{Pv} was determined from arrival times of the wave at adjacent sensors. Arrival of the P_v wave was interpreted as the first departure in the vertical geophone output in each 3-D sensor. Identification of the P_v-wave arrival times for the Sensor 2 – Sensor 3 pair and an example calculation of V_{Pv} are shown in Figure 4a for a static load of 44.5-kN. Based on a plane wave approximation (discussed in Section 4.2), the average strain induced by the transient downward hammer impact was about 0.00011%.

3.2. P_v-Wave Velocities from Steady-State Tests Using "Thumper"

When the geophone array was subjected to 10 cycles of vertical dynamic loading from "Thumper," there was an observed transient portion in the signals recorded by each 3-D receiver. This transient portion occurred during the initial "ramp-up" of the shaker to the desired load amplitude and generally lasted about 4 cycles. There was also a transient portion after the shaker was turned off which lasted about 2 cycles (see Figure 5). After about 5 cycles, the signal amplitude was generally stable, and so this portion of the response was assumed to represent steady-state conditions. A best-fit sinusoidal curve was fitted to cycles 7, 8, and 9 of the raw signals as shown in Figure 4b, and the time between peaks of adjacent sensors was used to determine the travel time of the P_v wave between sensors.

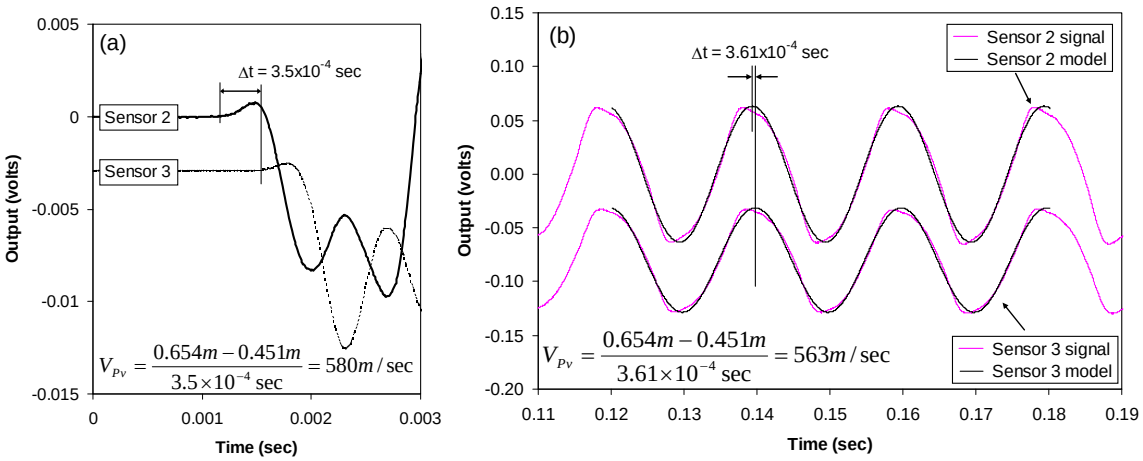

Figure 4. Determination of P_v-wave velocity between Sensors 2 and 3 under a 44.5-kN static load: (a) for transient, small-strain testing and (b) when subjected to a steady-state, dynamic load of +/- 1.1 kN driven at an excitation frequency of 50 Hz

3.3. Determination of Axial Strain by Displacement-Based Method

The axial strain, ε_a, between sensors was determined using a two-node, displacement-based method developed by Rathje et al. (2004) as:

$$\varepsilon_a = \frac{\Delta L}{L} \tag{3.1}$$

where ΔL is the change in distance between sensors due to dynamic excitation, L is the original distance between sensors, and strain is assumed to vary linearly between sensors. Since the geophones used in this study were velocity transducers, the displacement of the sensors was obtained by numerically integrating the velocity-time history once. After de-trending the displacement-time history of adjacent vertically-oriented sensors, the strain in the upward (positive) direction was often not the same as that in the downward (negative) direction. Therefore, the average of the upward and downward strains was assumed to represent the actual strain between the two sensors. This process is shown in Figure 5, where again this analysis is performed in the steady-state portion of the response.

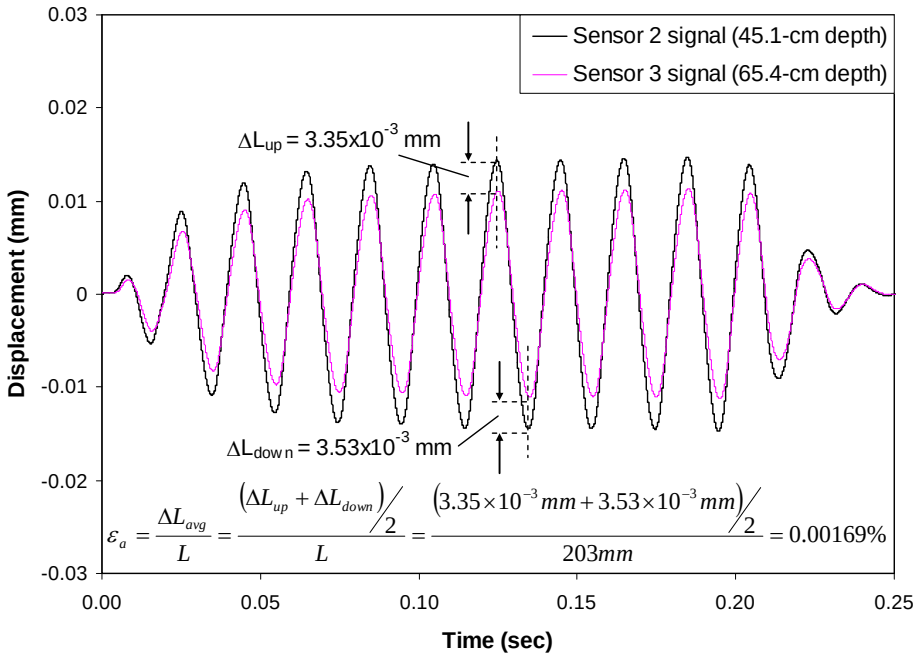

Figure 5. Determination of axial strain using displacement-time histories of adjacent sensors when subjected to a 44.5-kN static load and a steady-state dynamic load of +/- 1.1 kN driven at an excitation frequency of 50 Hz

To determine ΔL, it is critical that the displacement of each sensor be determined at the same instant in time. Therefore, in Figure 5 the maximum displacement (in the positive or negative directions) of Sensor 2 was first determined. Then the displacement of Sensor 3 was determined at the same time of the maximum displacement in Sensor 2 (note that this time is not the time at which the maximum strain occurs). However, due to the large number of data points collected during the dynamic tests, calculation of the entire strain-time history in order to extract the maximum strain was computationally expensive. Also, the difference between the strain calculated as explained above and the maximum strain determined using the entire strain-time history is approximately 20% based on preliminary analyses. This difference was considered insignificant given that axial strain is plotted on a logarithmic scale in Figures 8 through 10.

4. RESULTS

The results of the analyses described in the preceding section are presented below based on the signals from Sensors 2 and 3. Sensors 2 and 3 recorded the clearest signals at a frequency of 50 Hz, while the signal from Sensor 1 was erratic and difficult to interpret with confidence. The reason(s) for the poor performance of Sensor 1 are yet to be determined.

4.1. Variation of Small-Strain Wave Velocity with Confining Pressure

The small-strain P_v-wave velocities from the transient downhole tests were calculated following the procedure outlined in Section 3.1. These velocities are plotted versus the associated vertical stress level as open-diamond symbols in Figure 6 in terms of log V_{Pv} – log σ_v. The soil was expected to be highly overconsolidated due to an extensive period with no rainfall, though no measurements of pore water pressure were made. The small change in V_{Pv} with σ_v confirms this expectation and also shows that the loads used in this research were not sufficient to bring the soil to a normally consolidated state.

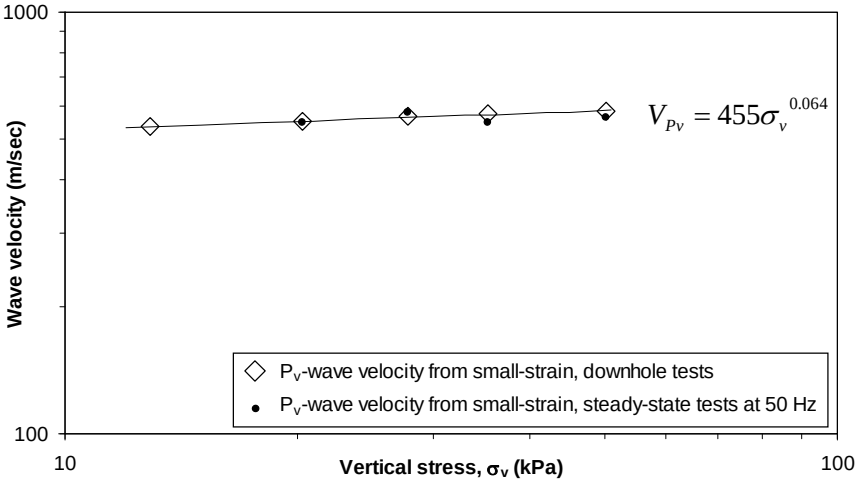

Figure 6. Variation of P_v-wave velocity with increasing vertical stress

P_v-wave velocities measured under the lowest dynamic load levels (hence, the smallest strain levels) in all four steps of Stage 1 are also shown in Figure 6. As seen, the P_v-wave velocities determined under steady-state, sinusoidal loading are close to the small-strain velocities from the traditional downhole measurements. This comparison was taken to confirm that the shaker generated constrained compression waves (not unconstrained compression waves) beneath the centerline of the baseplate of the shaker.

4.2. Evaluation of Linear and Nonlinear Constrained Moduli Using Steady-State Excitation

A comparison of the signals from the vertical and horizontal components of Sensors 2 and 3 is shown in Figure 7 for various levels of strain during Step 4 of Stage 1, i.e. Stage 1.4. At each strain level, the amplitude of the vertical component is approximately 9 to 10 times greater than either horizontal component, suggesting that the shakers induced primarily vertically propagating compression waves as hoped. At a dynamic load of +/- 1.1 kN (Figure 7a), the responses are symmetrical about zero, suggesting a linear system. At the +/- 7.6 kN-dynamic load (Figure 7b), the responses are no longer symmetrical and exhibit an accumulation of downward deformation. This change indicates the system is becoming slightly nonlinear. Finally, the responses at a dynamic load of +/- 13.3 kN (Figure 7c) are quite asymmetric and display significant accumulation of downward deformation, i.e. the system is exhibiting increased nonlinearity.

After the P_v-wave velocities under steady-state excitation were determined using the methods outlined in Section 3.2, the constrained modulus (M) was calculated using Richart et al. (1970) as:

$$M = \frac{\gamma_t}{g} V_{Pv}^{\ 2} \tag{4.1}$$

where γ_t is the total unit weight of the soil and g is acceleration due to gravity. The variation of M with axial strain is shown in Figure 8 for every load step in Stage 1. The small-strain constrained moduli calculated using Equation 4.1 and V_{Pv} from the small-strain, transient downhole tests are also plotted in Figure 8. The axial strains associated with these transient downhole tests were calculated assuming a plane stress wave travelling vertically through the system using Richart et al. (1970) as:

$$\varepsilon_a = \frac{\dot{z}}{V_{Pv}} \tag{4.2}$$

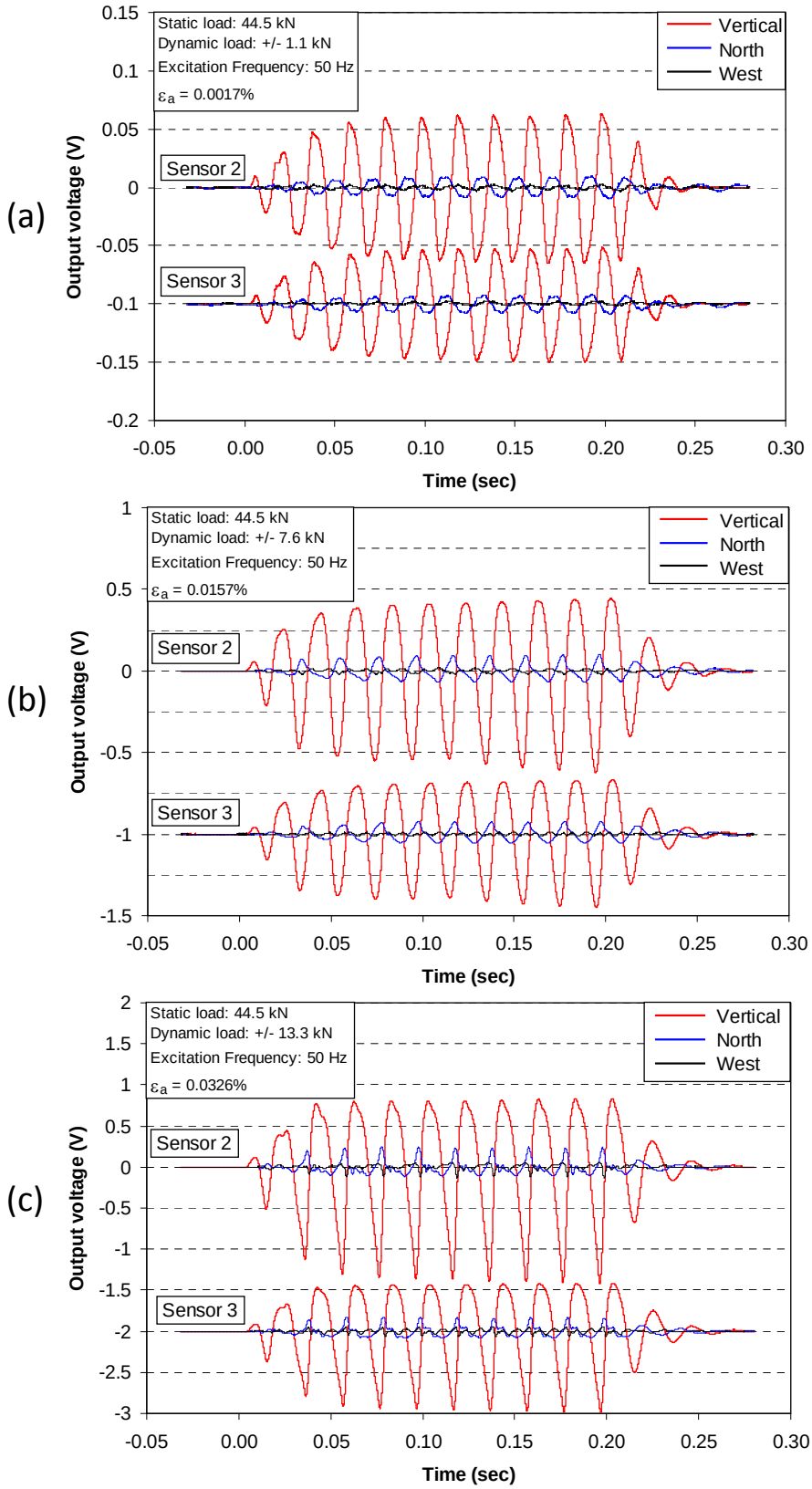

Figure 7. Outputs from the vertical and horizontal geophones in Sensors 2 and 3 at various levels of excitation during Stage 1.4: (a) ε_a = 0.0017%, (b) ε_a = 0.0157%, and (c) ε_a = 0.0326%

where $\dot{z}$ represents the maximum particle velocity in the vertical direction. The axial strains in these tests ranged from 0.00005 to 0.00017%. The average axial strain was about 0.00011% and was used to represent ε_a for all transient downhole tests. The nonlinear behavior of M is clearly seen in Figure 8 and is obviously quite complex. At the lowest confinement (σ_v ~ 20 kPa), the sandy silt exhibits an apparent dilatancy which results in M increasing with increasing ε_a over the strain range generated in these steady-state tests (ε_a = 0.0004 to 0.006%). At Stage 1.2, the dilatancy effect is smaller and is followed by a decrease in M at ε_a greater than about 0.008%. In Stages 1.3 and 1.4, M remains relatively constant until about 0.008% strain, after which M decreases with increasing ε_a. In Stages 1.2, 1.3, and 1.4, coupled nonlinearity and degradation created waveforms at the higher dynamic loads which are highly nonsymmetric (see Figure 7c). Therefore, these dynamic loads could not be analyzed using the sinusoidal curve-fitting method outlined in Section 3.2 and are not included in Figure 8.

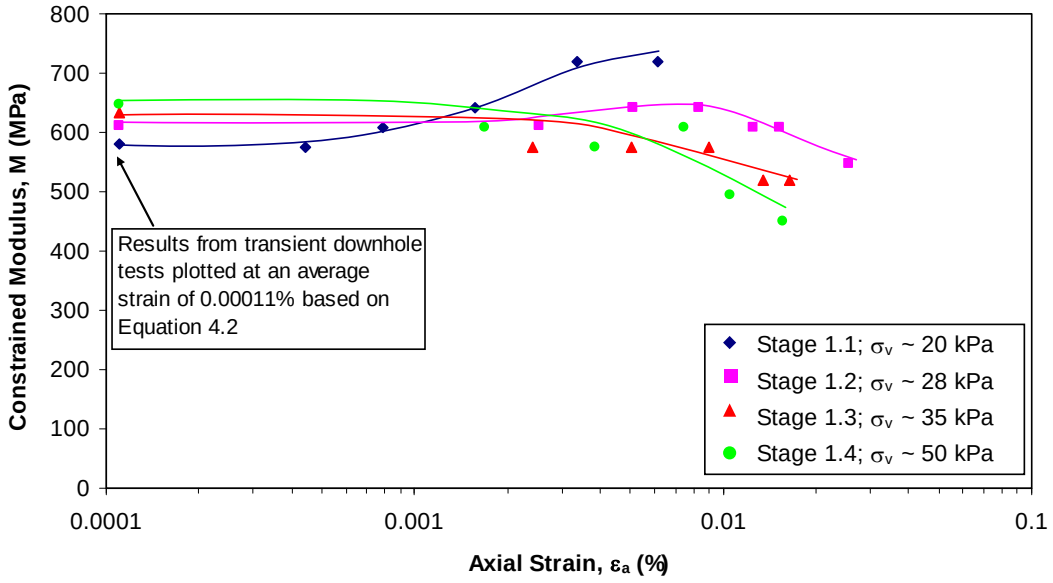

Figure 8. Variation of constrained modulus with axial strain for Sensors 2 and 3 (50-Hz excitation)

It is important to note that the results shown in Figure 8 are from the first set of tests ever conducted using the methods described in Section 2, and it is simply a hypothesis that dilatancy is occurring as mentioned above. Clearly, more work is needed to investigate this hypothesis. Moreover, the M – log ε_a curve is more nonlinear at the highest confinement (σ_v ~ 50 kPa) than it is at lower confinement states. This behavior of more strain dependency as ε_a increases has never before been observed and could possibly be due to several reasons including: (1) uncertainties in these new types of measurements and/or (2) degradation of the soil occurring at higher dynamic loads as shown by the downward movement in Figures 7b and 7c.

As traditionally done with G – log shear strain (γ) relationships, the M – log ε_a relationship at different pressures is presented as normalized constrained modulus (M/M_{max}) – log ε_a in Figure 9, where M_{max} is defined as the M from the transient, small-strain downhole tests. In Figure 9, the σ_v-dependent transition from M/M_{max} – log ε_a increasing with increasing axial strain to M/M_{max} – log ε_a decreasing with increasing axial strain is readily seen. The strain range where degradation seems to be contributing is also shown by the outlined zone in Figure 9.

A comparison of the data in Figure 9 with the M/M_{max} – log ε_a evaluated by Beresnev et al. (2002) based on weak and strong earthquake ground motions in the Japanese KiK-net accelerograph database is shown in Figure 10. Assuming the soil is constrained in the radial direction (and therefore the radial strain, ε_r, is zero), it can be shown using Mohr's circle for strain that the maximum shear strain, γ_{max}, in

a soil element is equal to the axial normal strain, ε_a. With this relation, a G/G_{max} – log γ curve is plotted on the same figure as the M/M_{max} – log ε_a curve. Umberg (2012) performed resonant column tests at confining pressures of 110 and 440 kPa on a soil composed of 50% silt and 50% sand. Based on these tests, Umberg's projected G/G_{max} – log γ curves for a 50-50 mixture of fine sand and silt at confining pressures of 20 and 50 kPa are also shown in Figure 10.

The M/M_{max} – log ε_a values reported by Beresnev et al. (2002) are generally near the lower bound of the M/M_{max} – log ε_a values determined in the present research, although the data from Beresnev et al. only extend to about 0.007% strain and occur at much higher stress levels. The Umberg (2012) G/G_{max} – log γ curves exhibit more nonlinearity than M/M_{max} – log ε_a.

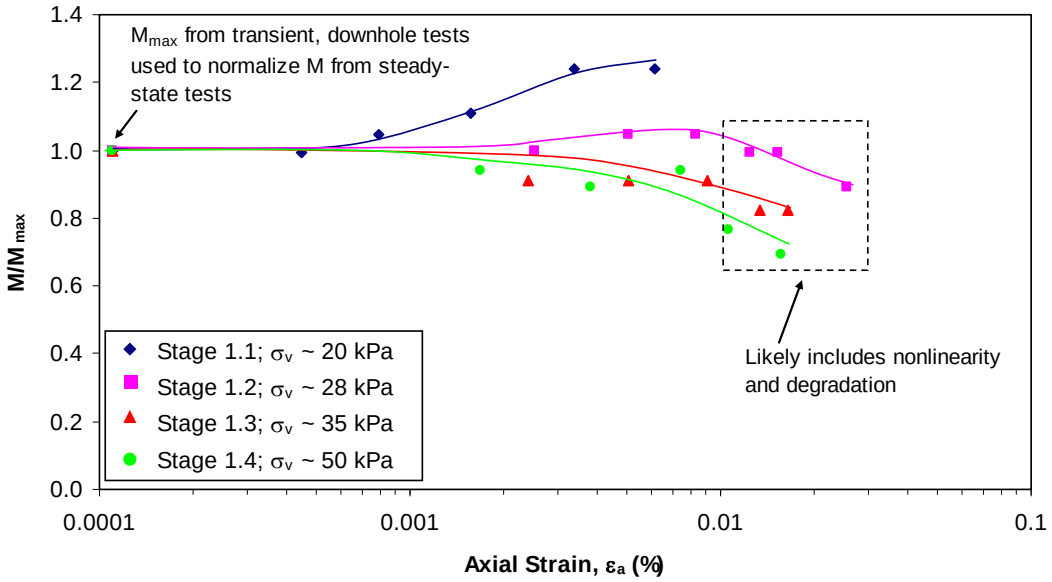

Figure 9. Variation of normalized constrained modulus with axial strain for Sensors 2 and 3 (50-Hz excitation)

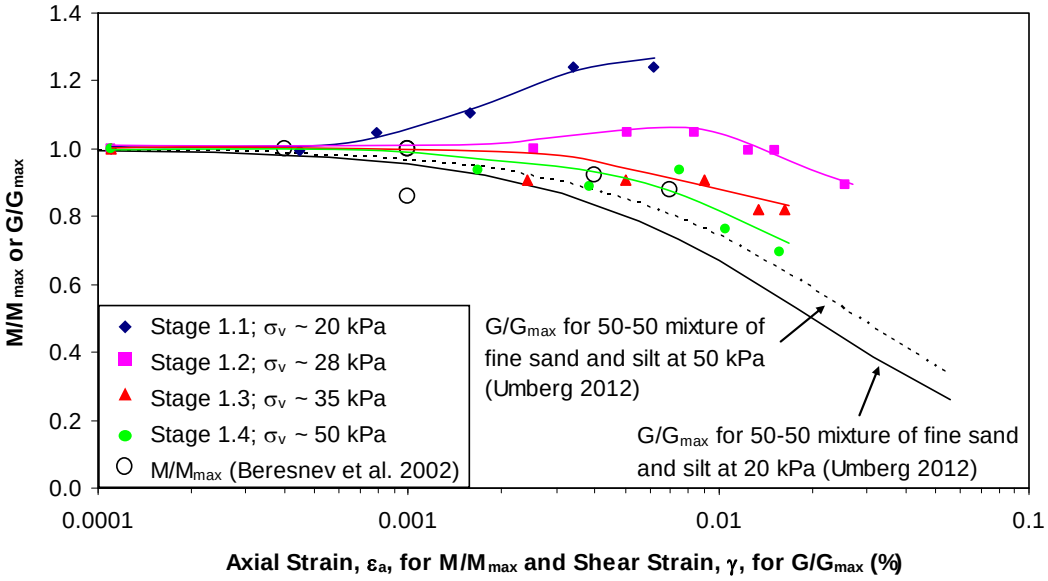

Figure 10. Comparison of nonlinear constrained and shear moduli

5. CONCLUSIONS

The testing program described herein involved field measurements of constrained compression waves in the small-strain (linear) and larger-strain (nonlinear) ranges. Field measurements were performed using: (1) a vertical array of 3-D geophone sensors buried in native soil and (2) stage loading above the array with static and dynamic loads applied with a large mobile shaker. The field method is promising in several key aspects. First, it is possible for the mobile shaker to induce vertically-propagating constrained compression (P_v) waves as confirmed by the good agreement between P_v-wave velocities from traditional small-strain, downhole tests and the steady-state, dynamic tests. Second, combined with traditional small-strain downhole seismic testing, use of the large mobile shaker permits P_v-wave measurements over a large range of axial strains in the soil and allows determination of both $M - \log \varepsilon_a$ and $M/M_{max} - \log \varepsilon_a$.

Although the testing procedure employed in this study is still under development, there are several limitations at this time. First, the confining pressures that were applied by the shaker are relatively low (about 50 kPa), and some means of increasing the pressure is needed. Also, there are very few data points in the axial strain range of 0.0001 to 0.001%, so the resolution is low in this strain range. Finally, the effects of soil type, spatial location of the geophones, and excitation frequency were not examined in the present research. Therefore, more extensive testing needs to be conducted in the future to investigate these factors and to refine the testing procedure.

Based on the measurements in this study, the shape of the $M/M_{max} - \log \varepsilon_a$ curves can be variable and quite complex. While this present research suggests that the $M/M_{max} - \log \varepsilon_a$ relationship may be more linear than the $G/G_{max} - \log \gamma$ relationship, the behavior of the $M/M_{max} - \log \varepsilon_a$ relationship already seems to be more complex than the $G/G_{max} - \log \gamma$ relationship.

ACKNOWLEDGEMENTS

Financial support for the study was provided by Los Alamos National Laboratory. Financial support for the development of the nees@UTexas equipment site was provided by the George E. Brown, Jr. Network for Earthquake Engineering Simulation (NEES) under grant CMS-0086605. The interaction and guidance of Dr. Ellen M. Rathje, Dr. Clark R. Wilson, Dr. Loukas F. Kallivokas, and Dr. Chadi El Mohtar are greatly appreciated. Additionally, thanks goes to the graduate students and staff at the University of Texas at Austin who assisted in the laboratory and field work, including Dr. Farn-Yuh Menq, Mr. Cecil Hoffpauir, Mr. Changyoung Kim, Mr. Curtis Mullins, and Mr. Robert Kent. Special thanks to Dr. Kevin Anderson and the Austin Water Utility – Center for Environmental Research for graciously allowing use of the Hornsby Bend site.

REFERENCES

Beresnev, I.A., Nightengale, A.M., and Silva, W.J. (2002). Properties of Vertical Ground Motions. *Bulletin of the Seismological Society of America.* **92:8**, 3152-3164.

Park, K. (2010). Field measurements of the linear and nonlinear shear moduli of cemented alluvium using dynamically loaded surface footings. Ph.D. Dissertation, The University of Texas at Austin, USA.

Rathje, E.M., Chang, W-J., Stokoe, K.H., II, and Cox, B.R. (2004). Evaluation of ground strain from in situ dynamic testing. *13th World Conference on Earthquake Engineering*. Paper No. 3099, Vancouver, Canada.

Richart, F.E., Jr., Hall, J.R., Jr., and Woods, R.D. (1970). Vibration of Soils and Foundations, Prentice-Hall, Upper Saddle River, NJ.

Stokoe, K.H., II, Kurtulus, A., and Park, K. (2006). Development of field methods to evaluate the nonlinear shear and compression moduli of soil. *Earthquake Geotechnical Engineering Workshop*, University of Canterbury, Christchurch, New Zealand, 15 pgs.

Stokoe, K.H., II, Rathje, E.M., Wilson, C.R., Rosenblad, B.L., and Menq, F.Y. (2004). Development of the NEES large-scale mobile shakers and associated instrumentation for in situ evaluation of nonlinear characteristics and liquefaction resistance of soils. *13th World Conference on Earthquake Engineering.* Paper No. 535, Vancouver, Canada.

Umberg, D.R. (2012). Dynamic properties of soils with non-plastic fines. M.S. Thesis, The University of Texas at Austin, USA.